

# Ara2: Exploring Single- and Multi-Core Vector Processing with an Efficient RVV1.0 Compliant Open-Source Processor

Matteo Perotti, *Student Member, IEEE*, Matheus Cavalcante, *Student Member, IEEE*,  
Renzo Andri, *Member, IEEE*, Lukas Cavigelli, *Member, IEEE*, and Luca Benini, *Fellow, IEEE*

**Abstract**—Vector processing is highly effective in boosting processor performance and efficiency for data-parallel workloads. In this paper, we present Ara2, the first fully open-source vector processor to support the RISC-V V 1.0 frozen ISA. We evaluate Ara2's performance on a diverse set of data-parallel kernels for various problem sizes and vector-unit configurations, achieving an average functional-unit utilization of 95% on the most computationally intensive kernels. We pinpoint performance boosters and bottlenecks, including the scalar core, memories, and vector architecture, providing insights into the main vector architecture's performance drivers. Leveraging the openness of the design, we implement Ara2 in a 22nm technology, characterize its PPA metrics on various configurations (2-16 lanes), and analyze its microarchitecture and implementation bottlenecks. Ara2 achieves a state-of-the-art energy efficiency of 37.8 DP-GFLOPS/W (0.8V) and 1.35GHz of clock frequency (critical path:  $\sim 40$  FO4 gates). Finally, we explore the performance and energy-efficiency trade-offs of multi-core vector processors: we find that multiple vector cores help overcome the scalar core issue-rate bound that limits short-vector performance. For example, a cluster of eight 2-lane Ara2 (16 FPUs) achieves more than 3x better performance than a 16-lane single-core Ara2 (16 FPUs) when executing a  $32 \times 32 \times 32$  matrix multiplication, with 1.5x improved energy efficiency.

**Index Terms**—RISC-V, Vector, ISA, RVV, Processor, Efficiency, Multi-Core.

## 1 INTRODUCTION

IN 1976, the Cray-1 supercomputer [1] achieved the world's top performance of 250 MFLOPS by exploiting Data Level Parallelism (DLP) through a vector Instruction Set Architecture (ISA). Almost half a century later, in 2020, another vector architecture took the highest spot in the TOP500 list by scoring around 537 PFLOPS of peak performance: the Fugaku supercomputer, based on Fujitsu's A64FX processor and Arm's Scalable Vector Extension (SVE).

Despite an increase in raw computer performance by nine orders of magnitude, today's computing systems struggle to meet the performance requirements of ubiquitous Artificial Intelligence (AI) and Machine Learning (ML) workloads. The amount of data to process grows faster than the technology-driven processing-speed gain [2], and the power required to sustain the ever-increasing performance needs is the main limiting factor from the cloud (operating cost, cooling) to the edge (battery lifetime, weight). It comes as no surprise that the quest for energy efficiency is crucial for today's computing systems [3] across all performance profiles, from supercomputers (Green500 ranking) to ultra-low power AI processors (MLPerf Tiny).

While the Cray-1 vector processor was conceived for pure performance in the heydays of Emitter-Coupled Logic (ECL) bipolar transistor technology, the recent feat of Fugaku proves that vector ISAs are well-positioned to answer the conflicting needs of rapidly increasing computational demands under a tightly-constrained power budget. First, they effectively address the Von Neumann Bottleneck (VNB) by reducing the number of instructions fetched from memory through the execution of the same instruction on multiple elements, in the so-called single instruction, multiple data (SIMD) execution model. Furthermore, vector processors leverage a Vector Register File (VRF) to enhance data reuse in computationally intensive applications while remaining vector-length agnostic, as the vector length can be programmed at runtime.

After the release of Arm's SVE and SVE2 vector ISAs, RISC-V also developed its RISC-V "V" (RVV) vector extension, getting much interest due to its openness and extensibility. RVV has reached frozen state with its 1.0 release in 2021 after six years of design and standardization efforts. Companies and academia developed numerous vector designs supporting various pre-release versions of RVV and targeting different application domains such as High-Performance Computing (HPC) [4], [5], [6], Deep Neural Networks (DNN) [7], AI/Augmented Reality (AR) [8], real-time applications [9], and Internet-of-Things (IoT) endpoints [10]. These designs are characterized by their heterogeneity in terms of deployed system architectures: [4], [5], [9], [11] are single-core systems, while [8], [10], [12], [13] are multi-core or multi-core-ready. Among them, [4], [9], [13] work with a relatively simple in-order core, while [5], [8], [10], [11],

- Matteo Perotti is with the Integrated Systems Laboratory (IIS), ETH Zurich, 8092 Zurich, Switzerland. E-mail: mperotti@iis.ee.ethz.ch
- Matheus Cavalcante is with the Electrical Engineering Department, Stanford University, California 94305, USA. E-mail: mcv@stanford.edu
- Renzo Andri and Lukas Cavigelli are with the Huawei Zurich Research Center. E-mail: {renzo.andri, lukas.cavigelli}@huawei.com
- Luca Benini is with the Integrated Systems Laboratory (IIS), ETH Zurich, Switzerland, and also with the Department of Electrical, Electronic and Information Engineering (DEI), University of Bologna, 40126 Bologna, Italy. E-mail: lbenini@iis.ee.ethz.ch.

[13], [14] deploy more aggressive superscalar or out-of-order scalar pipelines.

These designs show a wide spectrum of vector architectures, but there is a fundamental lack of detailed architectural performance studies on the effects that the design parameters of a vector processor (VRF organization and size, number of processing elements (PEs), target application vector length) and system configurations (scalar core, scalar caches, single- or multi-core configuration) have on the system’s performance and energy efficiency. As already noticed in [4], the scalar core can highly limit the system’s performance when processing short vectors. Moreover, despite the efforts to propose standard RVV benchmarks to ease architectural development and comparison [15], the aforementioned publications provide performance data only for, in the best case, a small set of kernels.

In the constellation of RISC-V-based Vector processor architectures, Ara [4] was among the earliest ones. Its internal number of Floating Point Units (FPUs) could be scaled from 2 to 16, and the design, implemented in a 22nm technology, reached 1 GHz in typical conditions in all the configurations, with a leading State-of-the-Art (SoA) of 41 DP-GFLOPS/W energy efficiency at its peak and 97% of FPUs peak utilization. The architecture, though, was compliant with only a limited set of RVV 0.5, the very first and preliminary version of RVV, missing key instructions like vector reductions, ubiquitous in the ML domain. The ISA architectural specifications and the software ecosystem deeply changed with the RVV updates, and RVV0.5-compliant designs are now obsolete.

In this paper, we present the RVV-1.0 Ara2 vector processor and leverage its efficient parametric architecture to explore a wide range of configurations to optimize computational efficiency. To our knowledge, Ara2 is the first open-source vector processor to support the specification RISC-V V 1.0. We analyze the frozen RVV specification and its major effects on the microarchitecture of a vector processor, highlighting the novelties/changes and the issues that arise from them.

Furthermore, Ara2 aims to close the gap between the various RVV architectures proposed throughout the years and the lack of thorough performance/efficiency analyses for microarchitecture and implementation. The key contributions of this work are:

- The Ara2 microarchitecture and design<sup>1</sup>, with support for the RISC-V “V” 1.0 ISA. We analyze the changes from the previous preliminary RVV specifications and discuss their impact on the system microarchitecture. To the best of our knowledge, Ara2 is the first open-source processor to support RVV 1.0.
- An in-depth analysis of performance depending on the application vector length on benchmark kernels from different application domains (Linear algebra, Digital Signal Processing (DSP), ML). Furthermore, we analyze the effect that the scalar processor and its memory system have on performance.
- An implementation of the Ara2 system in a 22nm Fully Depleted - Silicon on Insulator (FD-SOI) technology and its Power, Performance, Area (PPA) metric analysis from 2 to 16 lanes, with insights into the

impact that microarchitectural optimizations of the most critical all-to-all unit (Slide Unit (SLDU)) have on the scalability of the vector architecture.

- A performance/efficiency trade-off study on different hardware configurations, varying the number of vector cores and lanes per vector core on different problem sizes. We demonstrate how a multi-core vector architecture can mitigate the performance impact of the scalar core’s issue-rate limitation and identify the most efficient architecture for specific application vector lengths.

The paper is structured as follows: Sections 1 and 2 present an introduction and a background to contextualize the overall work. Section 3 discusses the main changes between RVV 0.5 and RVV 1.0, and Section 4 the implications on a lane-based vector processor, while, in Section 5, we present the updated architecture. In Section 6, we describe our experiment setup and describe the benchmark kernels used for our evaluations. Then, we present performance analysis, physical implementation results, and a performance/efficiency trade-off study on single- and multi-core architectures in Sections 7, 8, and 9, respectively. Finally, we provide a comparison with the state-of-the-art in Section 10.

## 2 BACKGROUND AND RELATED WORK

The vector processor architecture was first implemented by the Cray-1 supercomputer. A vector processor is characterized by its internal VRF, composed of a fixed number of registers whose size is upper-bounded by the ISA (usually with a very loose upper bound). Arm SVE and RVV feature 32 vector registers, each of which with a size from 128 to 2048 (SVE) or 64k (RVV) bits. The VRF can be conceptualized as L0 storage, meant to buffer data elements re-used multiple times close to the PEs<sup>2</sup> to avoid more costly memory accesses. Buffering more elements in the VRF lowers the pressure on the data memory [16]. The VRF, acting as an L0 buffer, also allows vector processors to be latency-tolerant with respect to memory stalls since every instruction occupies the PEs for multiple cycles. As noticed in [17], the tolerance against memory latency is generally higher when the architecture works on longer vectors.

Moreover, the vector architecture amortizes the instructions’ fetch, decode, and issue cost of each vector instruction by executing it on as many data elements as they fit in a vector register. Intuitively, the longer the vector, the less pressure on the instruction memory.

Two examples of successful commercial vector architectures are the NEC SX-Aurora TSUBASA and the Fujitsu A64FX. The latest generation of SX-Aurora TSUBASA belongs to the NEC SX architecture family and features a 16-nm technology 1.6 GHz 16-core architecture equipped with a 128-KiB VRF per core, composed of 64 vector registers connected to three 32-way Fused Multiply-Add (FMA) pipelines, totaling a peak performance of 192 DP-FLOP/cycle per core and 4.91 TFLOPs for the whole system. Instead, the 7-nm FinFET-technology A64FX is an Arm-SVE-based multi-core cluster-based architecture, where clusters of 13

1. <https://github.com/pulp-platform/ara>

2. With PE, we identify every execution unit within a vector architecture, e.g., FPU, Multipliers, Arithmetic-Logic Units (ALUs), etc.

TABLE 1: Overview of RISC-V Vector Processors.

Core Name	RVV version	Target	XLEN (bit)	float supp.	VLEN (bit)	Split VRF (lanes)	Open-Source
This work	1.0	ASIC	64	✓	1024 <sup>a</sup>	✓	✓
[14] SiFive P870	1.0	ASIC	64	✓	128	?	✗
[8] SiFive X280	1.0	ASIC	64	✓	512	?	✗
[13] SiFive P270	1.0rc	ASIC	64	✓	256	?	✗
[11] Andes NX27V	1.0	ASIC	64	✓	512	?	✗
[6] S.D. VU	1.0	ASIC	64	✓	128-4096	✓	✗
[12] Spatz	1.0 <sup>e</sup>	ASIC	32	✗	128-512	✗	✗
[9] Vicuna	0.10	FPGA	32	✗	128-2048	✗	✓
[7] Arrow	0.9	FPGA	32	✗	?	✓ <sup>b</sup>	✗
[18] Johns et al.	0.8	FPGA	32	✗	32	✗	✗
[5] Vitruvius+	0.7.1	ASIC	64	✓	16384	✓	✗
[10] XuanTie 910	0.7.1	ASIC	64	✓	128 <sup>a</sup>	✓	✗ <sup>c</sup>
[19] RISC-V <sup>2</sup>	?	ASIC	?	✗	256	✗	✓ <sup>d</sup>
[4] Ara	0.5	ASIC	64	✓	4096 <sup>a</sup>	✓	✓
[20] Hwacha	Non-Std.	ASIC	64	✓	512 <sup>a</sup>	✓	✓

<sup>a</sup> VLEN per lane.<sup>b</sup> VRF is split horizontally.<sup>c</sup> The vector unit is not open-source.<sup>d</sup> The scalar core is not open-source.<sup>e</sup> Limited subset of RVV.

cores (core-memory groups) are individually coupled with 8-GiB HBM2 modules and are connected together through a TofuD network on chip (NoC) interconnect, with a peak theoretical performance of almost 3.38 TFLOPs. All non-RISC-V vector architectures are commercial products and the microarchitectural details remain trade secrets. On the other hand, Table 1 summarizes the SoA of the RISC-V-based processors, which have been developed by companies as well as researchers. Ara2 is the first processor that supports RVV 1.0 (Vicuna [9] does not implement the floating-point and is only compliant with the Zve32x subset).

Among these vector architectures, [6], [8], [11], [12], [13], [14], are multi-core or multi-core-ready, testifying the interest of industry towards coupling the two paradigms. Section 10 provides a quantitative comparison of our design and the architectures in Table 1.

### 3 THE EVOLUTION OF RISC-V V

The RVV extension adds a VRF composed of 32 vector registers, which can individually buffer vector elements of the same type (e.g., FP32). The ISA includes element-wise operations between different vectors, reductions of vectors to a single scalar element, and predicated execution to implement simple control flows, i.e., the computation can be enabled/disabled with a single-element granularity.

RVV was first proposed in 2015 [21] and went through several revisions before becoming stable, which were initially not clearly formalized [22], [23], [24]. We refer to the last informal specification (2018) as v0.5, as done in [4].

The specification has now reached v1.0 frozen status. While the fundamental concept of RVV has remained consistent over time, three major differences deserve to be discussed: 1) the organization of the vector register file, 2) the encoding of the instructions, and 3) the organization of the mask registers.

#### 3.1 Vector Register File

**VRF state:** The VRF is an additional level in the memory hierarchy to buffer the vector operands. When the supported vector length is wide, it is usually implemented with Static

Random-Access Memories (SRAMs), and its byte layout highly impacts the architecture design.

v0.5: The register file had both a global and local state. Users could dynamically enable registers, and the hardware calculated the maximum vector length by distributing the byte space among the enabled registers. Each register could be individually programmed for various data types.

v1.0: The register file state is global. The vector register file consists of 32 VLEN-bit vector registers, where VLEN is a parameter specific to the implementation, representing the bit width of a single vector register (in RVV,  $VLEN \leq 2^{16}$ ). The granularity of the register file can be adjusted by configuring the parameter LMUL; for example, setting LMUL to 2 results in sixteen  $2 \times VLEN$ -bit vector registers. Moreover, the register file is agnostic on the data type of the stored elements.

**Striping distance:** The initial proposal did not provide strict constraints on the byte layout of the vector register file. This was specified later, and with the introduction of the striping distance (SLEN) parameter, it became especially lane-friendly in version 0.9 of the specifications.

v0.9:  $SLEN \leq VLEN$ : each vector register can be divided into a total of  $VLEN/SLEN$  sections with SLEN bits. Consecutive vector elements are mapped into consecutive sections, wrapping back around to the first section until the vector register is full [25].

v1.0:  $SLEN = VLEN$ : the VRF is considered a contiguous entity, and consecutive element bytes are stored in consecutive VRF bytes.

### 3.2 Instruction Encoding

v0.5: The instruction encoding was polymorphic, as the data type of the vector elements was set for each vector register. For example, the instruction `vadd` was used for both integer and floating-point vector additions.

v1.0: The encoding is monomorphic, and there are different instructions for different data types, i.e., integer, fixed-point, and floating-point. Consequently, the ISA has more instructions, becoming one of the largest extensions in the RISC-V ecosystem.

### 3.3 Mask Vectors

Vector processors run conditional code through predication, which, in RVV, is implemented by means of mask vectors, each containing one bit per element. When the operation is masked, the core executes on element  $i$  only if the  $i$ -th mask-vector bit is asserted.

v0.5: Each element of a mask vector could host one mask bit in its Least Significant Bit (LSB), and there were no instructions to manipulate mask vectors.

v1.0: Every register of the VRF can host a mask vector, and the mask bits are sequentially packed one bit after each other, starting from the LSB of the vector register. There are logical instructions to manipulate mask vectors.

## 4 RISC-V V AND LANES

In this section, we discuss the impact of the RVV extension on the microarchitecture. We will consider Ara as an example

of a design tuned to RVV 0.5, even if the discussion is not limited to it, while Ara2 is our new architecture.

Ara2 is a modular architecture with parametric VLEN targeting high performance and efficiency on a broad range of vector lengths. For example, with  $VLEN = 4096$ , the unit can process vectors up to 4 KiB, when  $LMUL = 8$ , with a 16 KiB VRF. Pushing for high vector lengths has many advantages: operating on vectors that do not fit the VRF requires strip-mining with its related code overhead, which translates into higher bandwidth on the instruction memory and more dynamic energy spent in decoding and starting the processing of the additional vector instructions. In addition, longer vectors help tolerate the memory latency [17] and the setup time of each vector instruction.

#### 4.1 VRF and Lanes

In Ara2, as in Ara, each lane contains a chunk of the distributed VRF, implemented with 8 1RW SRAM banks per lane. In the following, we motivate the distributed approach by comparing it with the alternative implementation, i.e., a monolithic VRF, which would make the VRF interconnect complexity grow with the square of the number of lanes  $\ell^2$ .

In general, the area of a crossbar ( $A_{\text{xbar}}$ ) is proportional to both the number of masters and slaves, as it requires *Masters* de-multiplexers and *Slaves* arbiters. With a split VRF, all the functional units of a lane (masters,  $M_{\text{lane}}$ ) connect to all the lane banks ( $B_{\text{lane}} = 8$ ), so the total interconnect area is the interconnect area of one lane multiplied by the number of lanes ( $\ell$ ),

$$A_{\text{xbar}}^{\text{split}} \propto M_{\text{lane}} \times B_{\text{lane}} \times \ell = M_{\text{lane}} \times 8 \times \ell, \quad (1)$$

while a monolithic VRF would connect all its banks ( $B_{\text{tot}} = 8 \times \ell$ ) to every master of each lane,

$$A_{\text{xbar}}^{\text{mono}} \propto (M_{\text{lane}} \times \ell) \times B_{\text{tot}} = M_{\text{lane}} \times 8 \times \ell^2. \quad (2)$$

The quadratic dependency on the number of lanes limits the scalability of a vector processor based on a monolithic VRF. Moreover, the split VRF allows for more freedom on the macro placement during floorplanning and better routability since the interconnect is local to each lane.

#### 4.2 Byte Layout

With RVV 1.0, the VRF byte layout is the same as the memory byte layout, i.e., byte  $i$  of a vector in memory is kept in byte  $i$  of the VRF. This can be sub-optimal in the case of a laned vector processor. Indeed, not to complicate mixed-width operations and to maximally exploit DLP, Ara2 maps consecutive elements to consecutive lanes, i.e., element  $i$  is kept in lane  $i \bmod \ell$ . In this case, depending on the Element Width (EW), the same byte can be mapped to different lanes, as summarized in Figure 1.

As a consequence, the processor must track the last EW with which each vector register was written, to be able to restore its content, and the units that access a vector register must be able to re-map its elements.

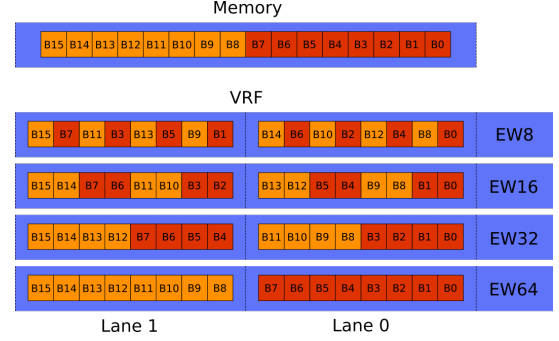


Fig. 1: 2-lane Ara2 VRF byte layout for different data widths.

#### 4.3 Shuffle/Deshuffle

The remapping is realized with shuffling (bytes to VRF) and deshuffling (bytes from VRF) logic, which translates into a level of byte multiplexers, one per output byte. With  $L$  lanes with a 64-bit datapath each, a unit that accesses the VRF can shuffle/deshuffle  $L \times 8$  bytes every cycle by using  $L \times 8$  multiplexers. Since an RVV unit should support EWs of 8, 16, 32, and 64 bits, each multiplexer has four input bytes.

#### 4.4 RVV 1.0 Implementation Challenges

Supporting RVV 1.0 with a lane-based architecture poses non-trivial challenges:

**Source Registers** Every time a source register is read with an  $EW_{vs}^{\text{new}}$  different than its previously encoded  $EW_{vs}^{\text{old}}$ , Ara2 should reshuffle its bytes to reinterpret its content according to the new element width. Generally, if the operation is executed outside of the lanes, the units can automatically reshuffle the data elements on the fly. In the case of in-lane operations, the SLDU should reshuffle the source register content since, with a different EW, bytes belonging to the same element can be in different lanes. We do this by injecting a reshuffle operation before the “offending” instruction.

**Destination Registers** RVV also mandates to support a tail-undisturbed policy. When in place, the destination elements past the last active one should not be modified. When an  $EW_{vd}^{\text{new}}$ -instruction writes a vector register  $vd$  previously encoded with  $EW_{vd}^{\text{old}} \neq EW_{vd}^{\text{new}}$  and the old content of  $vd$  is not fully overwritten, the unmodified bytes get corrupted since the byte mapping of  $vd$  is no longer unique.

To avoid corrupting the tail elements, when this situation occurs, Ara2 should deshuffle the destination register using  $EW_{vd}^{\text{old}}$  and reshuffle it back using  $EW_{vd}^{\text{new}}$  by injecting a reshuffle operation (i.e., a vector slide with null stride) into the SLDU before the offending instruction. Since it is not possible to know how many bytes need to be reshuffled unless both the vector length and the element widths are dynamically tracked for each vector register, the reshuffle acts on the whole register. No reshuffle is injected when the offending instruction writes a whole vector register, as reshuffling hurts the Instructions Per Cycle (IPC) if its latency cannot be hidden and if this operation causes structural hazards on following slide or reduction instructions.

Reshuffling is costly, as the offending instruction has a read-after-write (RAW) dependency on the reshuffle. The compiler can alleviate the problem by assigning EW-encoded vector registers to instructions with the same EW.

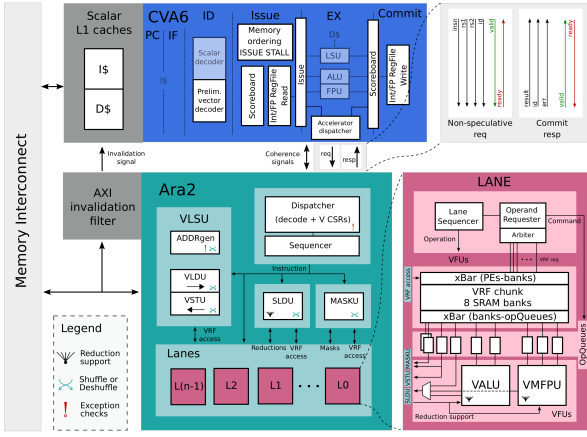


Fig. 2: Top-Level block diagram of the Ara2 system with the vector co-processor (green), a more detailed diagram of the lane (magenta), and the host scalar core CVA6 (blue).

## 5 ARCHITECTURE

In Figure 2, we show the block diagram of the scalar core CVA6 and the vector unit Ara2. The architecture is based on Ara [4], with the following major enhancements:

**Decoding:** With the new RISC-V V specifications, the encoding of the vector instructions now fully specifies the data type of the vector elements on which the instruction operates. This allows moving most of the decoding logic and vector-specific Control and State Registers (CSRs) from CVA6 to the vector unit, making CVA6 more agnostic on the V extension. In the updated architecture, CVA6 keeps only the pre-decoding logic strictly needed to know 1) if the instruction is a vector instruction (to dispatch it to the vector unit when it reaches the head of the scoreboard), 2) if the vector instruction is a memory operation (to enforce cache coherence), and 3) if the instruction needs a scalar value from the integer or floating-point scalar register files.

**CVA6-Vector Unit Interface:** The interface between the host processor CVA6 and the vector unit is generalized: the unit is implemented as a modular accelerator with its own CSR file. While decoding, CVA6 identifies vector instructions, pushes them to a dispatcher queue, and dispatches them to the accelerator once they are no longer speculative.

**Memory Coherence:** CVA6 and the vector unit have separate memory ports, and CVA6 has a private L1 data cache. At the same time, the RISC-V ISA mandates a strictly coherent memory view between the scalar and vector processors. Ara [4] violates this requirement and needs explicit memory fences that write back and invalidate the CVA6 data cache between accesses on shared memory regions, adding a significant performance overhead and reducing code portability. In Ara2, we develop a hardware mechanism to ensure coherence. We adapt the CVA6 L1 data cache to a write-through policy so that the main memory, which is accessed by the vector unit as well, is always up-to-date. When the vector unit performs a vector store, it invalidates the corresponding cache lines in the CVA6 data cache. Moreover, we issue 1) scalar loads only if no vector stores are in-flight, 2) scalar stores only if no vector loads or stores

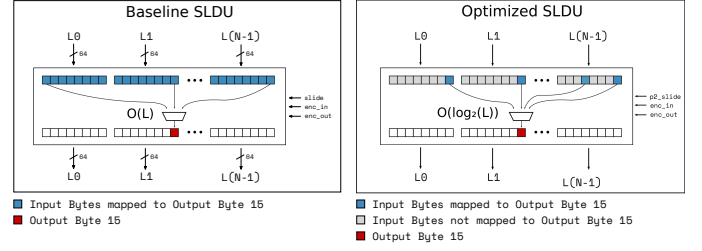


Fig. 3: Comparison between the baseline and the optimized slide units, with a focus on how an arbitrary byte (15th) is mapped to the input bytes. The baseline slide unit supports arbitrary slide amounts and can slide and re-encode a vector in the same cycle. Each output byte is mapped to every input byte, so that the total number of connections is  $O(L^2)$ . In the optimized design, we support only power-of-two slides. Moreover, slides and re-encoding cannot happen at the same time. The total number of connections grows following an  $O(L \times \log_2(L))$  behavior.

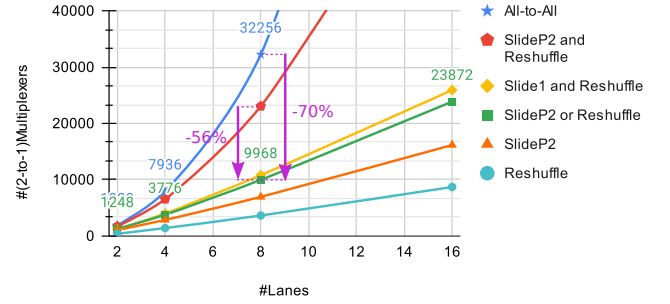


Fig. 4: Number of 2-to-1 multiplexers needed to implement a slide unit as a function of the number of lanes with different configurations. An all-to-all slide unit connects every input byte to every output byte and supports every slide and reshuffle operation in one cycle. Other configurations support only slides by powers of two (SlideP2), slides by one (Slide1), and can slide and reshuffle or either slide or reshuffle.

are in-flight, and 3) vector loads or stores only if no scalar stores are pending.

**Mask Unit:** After the update to RVV 1.0, the mask bits used by one lane can be stored in a different one. Thus, we designed a Mask Unit, which can access all the lanes at once to fetch, deshuffle at bit granularity, and dispatch the correct mask bits to each lane. Moreover, the Mask Unit (MASKU) combines the results of many vector mask instructions, such as `vcpop` and `vfirst`. The introduction of an additional unit that accesses all the lanes leads to a greater routing complexity, especially when scaling up the number of lanes, as already noticed in [4].

**Optimized Slide Unit:** The mask unit makes the physical implementation effort harder due to its all-to-all connections to/from the lanes. Reducing the complexity of each all-to-all connected unit is paramount to ease the physical implementation (placement and routing) of the system. A preliminary study of how the area of the system scales with the number of lanes shows that the most problematic block is the slide unit, being the largest all-to-all connected unit and scaling quadratically with the number of lanes. This is expected, as the block supports slides by arbitrary amounts for element widths down to 8 bits by mapping the  $8 \times L$  input bytes to the  $8 \times L$  output bytes. This interconnect can be simplified by limiting the type of operations supported by the unit. For example, we can constrain the datapath to support only slide-by-1 or slide-by-power-of-two slide



instructions, with the other strides handled with multiple micro-operations.

In Figure 4, we attach a plot showing the number of 2-to-1 multiplexers needed to implement the interconnect with different slide unit configurations. This number is also a lower bound to the number of wires that connect the input bits before the slide to the output slided bits and is a valid metric to estimate the area of the interconnect and the wiring complexity during the routing stage. Since non-power-of-two slides and reshuffling are uncommon, we limit the strides fully supported in hardware to powers of two and handle the remaining strides with micro-operations, saving up to 70% of the estimated area and wires, as shown in Figure 3.

**Reductions** Since our design has lanes, we implement reductions using a 3-steps approach: intra-lane, inter-lane, and SIMD reduction steps. The intra-lane reduction fully exploits the data locality within each lane, maximizing the ALU (or FPU) utilization and efficiency, reducing all the elements already present in the lane. The inter-lane reduction moves and reduces data among the lanes in  $\log_2(\ell) + 1$  steps,  $\ell$  being the number of lanes, using the slide unit; since there is a dependency feedback between the slide and ALU (or FPU) units, the latency overhead of the communication is paid at every step. Finally, the SIMD reduction reduces the SIMD word, if needed; therefore, its latency logarithmically depends on the element width.

Floating-point reductions need special care since the FPU is pipelined. To keep the throughput at its maximum, the internal pipeline registers of the FPU are used as accumulators. During the intra-lane phase and after adding the first two elements together, each FPU is constantly fed with one operand per cycle. The other FPU input is either a neutral value (zero for the addition) or one of the partial sums coming from the FPU output, when available. In the best case, after  $N/L$  cycles, each FPU pipeline register contains a partial sum, and the reduction will be completed in  $R \times (1 + \log_2[R]) - ([R] - R) - 1$  cycles. Here,  $N$  is the number of 64-bit packets of operands in the vector to reduce,  $L$  is the number of lanes, and  $R$  is the number of FPU pipeline stages. When  $R$  is a power of two, the formula simplifies to  $R \times (1 + \log_2(R)) - 1$ . Then, during both the inter-lane and SIMD reductions, the FPU latency directly affects each micro-operation. Since the number of FPU pipeline registers increases with the EW, reductions on lower bit widths can be faster than the ones on higher bit widths.

## 6 EXPERIMENT SETUP

In the following section, we describe our experiments in detail, including the system configuration, tools, and metrics used for performance characterization, physical implementation, and single-/multi-core trade-off evaluations. Then, we outline the details of our benchmark pools and the rationale behind selecting our kernels. In the following, we will use the term *system* to refer to the system-under-test composed of CVA6, its caches<sup>3</sup>, and Ara2. Ara2 and the L1 caches connect to a 1-cycle-latency SRAM memory<sup>4</sup> via the AXI memory interconnect shown in Figure 2. While analyzing a

complex memory hierarchy is out of the scope of this work, this simple configuration includes L1 caches and a standard system bus initiator.

**Performance analysis:** We characterize the system’s performance in terms of *raw throughput ideality*, which identifies the ratio between the measured raw throughput and the ideal maximum raw throughput achievable by the vector processor for a particular kernel. With *raw throughput*, we identify the ratio between the number of “useful” operations of an algorithm and the number of clock cycles spent to execute it, counted from the first vector instruction dispatched from CVA6 until the last vector instruction fully executed by Ara2 (*raw* since there is no frequency information). This metric helps study the ideality of the design on different vector lengths (different problem sizes). For our measurements, we run all benchmarks on our vector system using a cycle-accurate simulation, with all the benchmark instructions and data preloaded in the SRAM main memory.

We measure the performance of each benchmark for different vector lengths (from 32 to 1024 Byte) and hardware configurations (Ara2 with 2, 4, 8, and 16 lanes) to constitute a baseline for further performance analyses.

**What-if analyses:** We repeat the performance measurements by replacing CVA6 and its L1-caches with a FIFO that contains the whole dynamic vector instruction trace of the program in analysis and the correct scalar register file entries to be forwarded to Ara2 if needed. This allows us to determine the impact of the scalar part of the system on the overall computation and set an upper bound on performance gains achievable by streamlining the scalar subsystem. In these conditions, performance is only limited by the vector co-processor. Additionally, we track the number of L1-cache misses to study the effect of scalar memory system non-idealities on kernel performance. Finally, we further streamline the vector processor with modifications that would impact the vector processor hardware (e.g., by aggressively upsizing the internal queues and scoreboard) and study their impact on the system’s performance. The overall experiment highlights the bottlenecks that limit the computation performance and the cost to overcome them.

**Physical implementation analysis:** After synthesizing, placing, and routing the system in 22nm FD-SOI technology using industrial-grade tools, we evaluate its power, performance, and area (PPA) metrics. The system includes CVA6, its L1 caches, the invalidation filter, Ara2, and the interconnects up to the system crossbar. To analyze the switching activity of the netlist internal signals, we use a cycle-accurate simulator to generate a VCD file with delay back-annotations from the physical place-and-routed design. We repeat the analyses for systems with 2, 4, 8, and 16 lanes. The input matrices are samples from a uniform distribution over  $[0,1)$ .

**Multi-Core analysis:** The system is modified to accommodate multiple clusters of the previously implemented system, and the SRAM main memory is multi-banked to support multiple Ara2 instances, with one bank per Ara2 and every bank with a parallelism of  $4 \times L$  Byte each, with  $L$  being the number of lanes of each Ara2. Moreover, we implement a lightweight synchronization engine via system-level CSRs to let the clusters synchronize at the end of the execution. The main objective is to evaluate the impact of the multi-core vector architecture on performance and energy efficiency.

3. I\$: 4 KiB, 4 sets, 128-bit line. D\$: 8 KiB, 4 sets, 256-bit line

4. Memory: 2M words,  $4 \times L$  Byte/word,  $L$  being the number of lanes

TABLE 2: Benchmarks used in the performance analysis.

Program	Domain	DType	CB	M	S	SMO	IMO	R	Max Perf. [FLOP/cycle]
<b>matmul</b>	Linear Algebra, ML	FP64	Y	N	N	N	N	N	$1 \times 2.0 \times L$
<b>conv2d</b>	Signal Processing, ML	FP64	Y	N	Y	N	N	N	$1 \times 2.0 \times L$
<b>dotproduct</b>	Linear Algebra	FP64, int64	N	N	N	N	N	Y	$1 \times 0.5 \times L$
<b>jacobi2d</b>	Stencil	FP64	Y	N	Y	N	N	N	$1 \times 1.0 \times L$
<b>dropout</b>	ML	FP32	N	Y	N	N	N	N	$2 \times 0.25 \times L$
<b>fft</b>	Signal Processing	FP32	Y	Y	Y	N	Y	N	$2 \times 5/4 \times L$
<b>dwt</b>	Signal Processing	FP32	N	N	N	Y	N	N	$2 \times 0.5 \times L$
<b>pathfinder</b>	Routing Algorithm	int32	N	Y	N	N	N	N	$2 \times 1.0 \times L$
<b>exp</b>	Scientific, ML	FP64	Y	N	N	N	N	N	$1 \times 28/21 \times L$
<b>softmax</b>	ML	FP32	Y	N	N	N	N	Y	$2 \times 32/25 \times L$
<b>roi-align</b>	ML	FP32	N	N	N	N	N	N	$2 \times 3/5 \times L$

CB: Compute Bound, M: Masks, S: Slides, SMO: Strided Mem. Ops., IMO: Indexed Mem. Ops., R: Reductions

To do this, we vary the number of cores per cluster, the number of lanes of each vector core, and the application vector length of the floating-point matrix multiplication algorithm. The modified kernel used in this phase is slightly different from the one used in Section 7, and scalar caches are not warmed up to ease the automatic VCD dumping script. However, the comparison is still fair as all the configurations run the same program.

We insert a synchronization point before and after the kernel execution, measure performance and energy efficiency within this time span, and simulate `fmatmul` between square matrices with different sizes ranging from 4x4 to 256x256 elements on systems with {1, 2, 4, 8} cores and {2, 4, 8, 16} lanes, with no more than 16 FPU's in total.

**Benchmark selection:** Table 2 summarizes the benchmarks used to evaluate the Ara2 System's performance. The benchmarks include a mix of kernels from various domains, including signal processing, linear algebra (BLAS), and machine learning (ML). The kernels were chosen to stimulate all the main units of Ara2 and include both compute-bound and memory-bound kernels. Here is a brief overview of each benchmark:

`matmul` and `conv2d` are two compute-bound kernels that are used in multiple domains (Signal processing, linear algebra (BLAS), ML). Their performance behavior is crucial due to the kernels' ubiquity. We re-used `matmul` from [4], and optimized the 3x7x7-kernel `conv2d` by keeping, after the initial setup steps, seven output vectors in the VRF for every loaded input vector, to maximize data reuse. `fft` and `dwt` are well-known algorithms used in the signal processing domain. We implement a vectorized version of `fft` by exploiting the large Ara2 VRF to buffer all the input samples. This avoids costly transfers to and from memory, in a similar way as shown in Bertaccini et al. [26], and sets a limit to  $128 \times$  Lanes input samples (e.g., 2048 input samples with 16 Lanes). We take `pathfinder`, `jacobi2d`, and `exp` from the RiVec benchmark suite repository [15], [27], and optimize them with assembly instructions. We chose these three kernels from RiVec since they were the easiest ones to bring to bare-metal C code, as the suite was primarily developed to run on gem5 with OS support. We vectorized `dropout`, `roi-align`, and `softmax`, three kernels used in the ML domain, and we included `dotproduct` since it does not expose multiple dimensions for parallelization and forces the implementation to use a reduction.

## 7 PERFORMANCE CHARACTERIZATION

In this section, we analyze the system's performance and how it changes with the system configuration, the scalar core,

the configuration of the scalar memory hierarchy, the number of lanes, and the application vector length.

### 7.1 Lanes and Vector Length

When we scale up the Ara2 co-processor by doubling its number of lanes, we also double 1) its AXI bus data width and 2) the parallelism of the all-to-all internal units (MASKU, SLDU, Vector Load/Store Unit (VLSU)). For a deeper understanding of the performance scalability, Figure 5 shows the correlation between the performance ideality of the Ara2 co-processor, its number of lanes, and the application vector size, for two different kernels: `dotproduct` and `fmatmul`. Specifically, on the  $x$ -axis of the plots, we list different vector sizes (in Byte), i.e., the number of vector elements times the element size. For example, the entry (8L, 512 Byte) corresponds to the performance ideality achieved by an 8-lane system when dealing with vectors composed of 64 64-bit elements each. When the ratio #Byte/#Lane is constant, the achieved performance ideality is similar for systems with different configurations. This means that the raw throughput almost doubles when the number of lanes doubles if the number of elements per lane is constant. This experiment shows that the computation ideality of Ara2 is related to the ratio between the application vector length and the number of lanes and that a vector is *short* or *long* only depending on the vector architecture on which will be processed. On the right, the two heat plots visually remark the same concept, as entries on the same diagonal (same byte-per-lane ratio) have similar colors, i.e., similar performance.

Both analyzed kernels show a slight performance regression for a constant byte-per-lane ratio. In the case of the `dotproduct`, the performance decreases when increasing the number of lanes because of the vector reduction instruction, whose latency depends on the number of lanes during the inter-lane phase. On the other hand, `fmatmul` is computed on square matrices, and when the matrix size increases, the arithmetic intensity increases as well. Moreover, the performance drop of the 2L configuration at 16 and 32 Byte/Lane testifies that when the number of elements is too low, the setup time of the kernel is less amortized.

### 7.2 Baseline System's Performance

Figure 6 presents the performance ideality of the baseline system across all benchmarks in our pool, varying the application vector length. The darker the green shades in the plot, the closer the system performance is to the ideal. As noticed in Section 7.1, the ratio between the vector length and the number of lanes significantly affects performance, as shown by the 2-lane design reaching over 70% of average performance ideality with a 1KiB vector (512 Byte/lane), while the 16-Lane system, with the same vector, would reach only 33% (64 Byte/lane). This is apparent in the heatmaps, where the darker colors shift right by one position every time the lanes double.

`fft`, `dwt`, `softmax`, and `pathfinder` perform below average, even for high ratios of Byte/lanes, with `softmax` suffering from the floating-point division data-dependent latency and the large setup time for preloading the approximation function coefficients of the software-emulated exponentiation. `dwt` is slowed down by misaligned strided

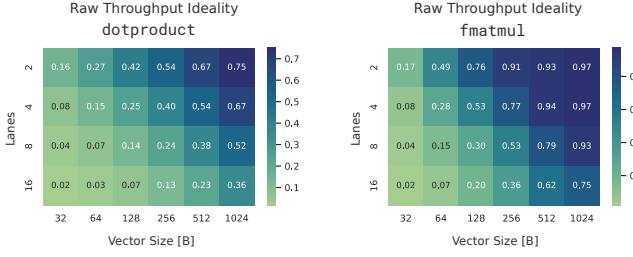


Fig. 5: Correlation between Raw throughput Ideality and Byte/lane ratio for dotproduct (top) and fmatmul (bottom). The raw throughput ideality tends to be similar when the number of elements per lane is the same (on the diagonals).

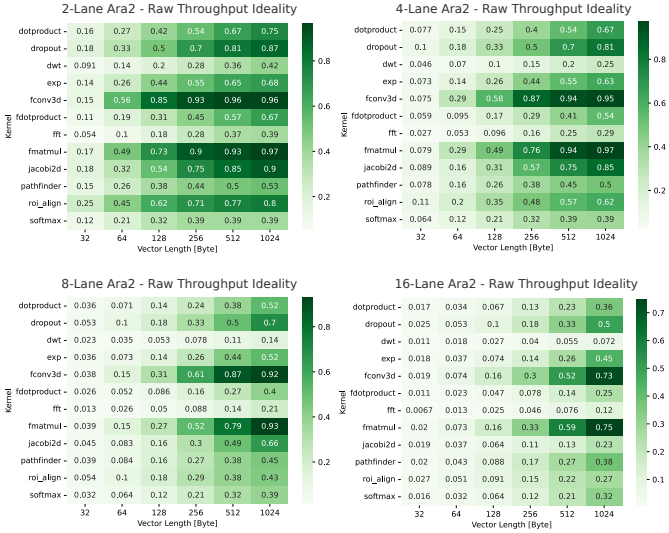


Fig. 6: Performance evaluation of the system with different configurations and number of lanes on different kernels and vector lengths.

memory accesses, and `fft` by the indexed stores at the end of the program. However, even considering these slower kernels, the system achieves, on average, 50% of its raw throughput ideality on all the kernels and configurations starting from 128 Byte/Lane.

The Ara2 system achieves higher performance at lower byte-per-lane ratios with the most crucial kernels like `fconv2d` and `fmatmul`, reaching over 95% of its maximum theoretical throughput starting from 128 Byte/Lane, or 75% from 64 Byte/Lane.

### 7.3 Ideal Dispatcher System's Performance

Replacing the scalar core (CVA6) with an ideal dispatcher idealizes the scalar core, its memory system, and the non-vectorial code. In this way, we can trace an upper bound to the available performance achievable through the Ara2 system alone, abstracted from the scalar subsystem. With an ideal dispatcher, the performance is no longer limited by the issue-rate limitation described in [4], and CVA6 cannot interfere with Ara's memory transfers.

Figure 7 shows, for the 2- and 16-Lane system, the raw throughput ideality gain we get by replacing CVA6 with an ideal dispatcher. We report the plots for 64, 256, and 1024 elements. The yellow lines track the number of scalar

L1I-cache and L1D-Cache misses during the vector program computation, from the first vector instruction to the last one.

When the number of Bytes per lane is lower than 8 (e.g., 16-Lane Ara2 - 64B), the effective number of lanes is reduced for 64-bit data kernels since there are not enough elements to fill all the lanes, and the real maximum performance achievable is the maximum performance multiplied by the number of elements per lane. In this condition, the performance is not limited by CVA6.

When the number of Bytes per lane is lower than 64 (2-Lane Ara2 - 64B and 16-Lane Ara2 - 256B), the effective number of banks used in each lane is reduced from eight to the number of elements per lane for the 64-bit data kernels, especially if we do not implement a Barber Pole's VRF layout. For example, if the vector length is 128B and the system has 16 lanes, only one bank per lane is effectively used; all the read and write operations will target the same bank in each lane, increasing the probability of conflicts. Since multiple PEs experience a stall when they try to access the same bank simultaneously, and the conflict probability grows when we reduce the number of banks, these configurations are slowed down by more bank stalls. The lower the byte-per-lane ratio, the more impact a bank stall will have on the final runtime.

In this region, we see that some kernels moderately benefit from the ideal dispatcher. This also happens when the number of elements grows until the number of byte-per-lane becomes sufficiently long to peak performance, and the non-idealities of the scalar core and memory system are almost completely amortized by Ara.

`fmatmul`, `fconv2d`, and `jacobid2d` greatly benefit from the ideal dispatcher, showing a correlation between the D-Cache misses and their performance increase when CVA6 is replaced with an ideal dispatcher. To prove the correlation, we simulate the three kernels on a 16-Lane System with 128 elements (1024 Byte), idealizing the cache system so that it always hits. Figure 8 shows the results. With an ideal cache system, the three kernels virtually perform as when executed by the ideal-dispatcher system, which shows the importance of the scalar memory system for kernels that heavily rely on operand forwarding between the scalar and the vector core. Instead, `exp` and `roi-align` slightly benefit from the ideal dispatcher because of the non-negligible amount of housekeeping scalar code in the program.

### 7.4 Further Performance Considerations

In the following paragraphs, we discuss the effect of further system/level and microarchitectural modifications used in vector processors that can impact performance and identify the main performance drivers that can boost the system's performance with low Byte/Lane ratios.

#### 7.4.1 VRF Layout

The current instance of Ara2 does not implement Barber's Pole VRF layout, which was originally introduced to avoid the initial stalls that every vector instruction with at least two source registers would experience [4]. These stalls are especially critical for short-vector applications where each vector instruction lasts for fewer cycles.

Barber's Pole does not always reduce the number of runtime stalls, though. Highly regular applications such as





Fig. 7: Scalar cache misses and performance gain when CVA6 is replaced by an ideal dispatcher, varying the number of lanes in the Ara2 system and the number of elements in the vector, measured in bytes.

#### Performance Impact of the Scalar Memory System

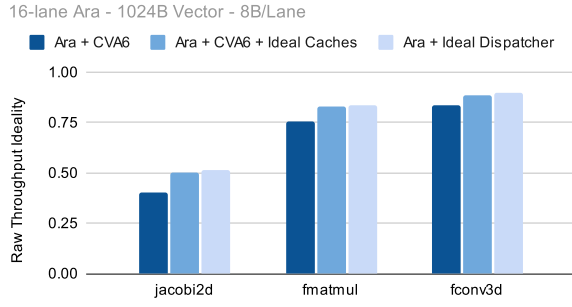


Fig. 8: Performance comparison of a 16-Lane System with 64B/Lane among three different configurations: a) Baseline System, b) Baseline System with ideal CVA6 data-cache, c) System with ideal dispatcher.

`fmatmul` suffer more stalls when implementing this byte layout and dealing with vectors that are sufficiently long to amortize the initial stalls. Without Barber's Pole, when an application is highly regular, and the vector processor receives enough computational vector instructions to keep its operand requesters busy, the VRF experiences a regular access pattern during execution, especially when the vector length is multiple of the number of banks in a lane. After the first stalls, the source operand requesters make their requests in an interleaved fashion, once per cycle, without conflicting anymore. When an instruction is over, and the next one starts, the pattern is preserved since the previous instruction issued its last request to the last VRF bank, while the next instruction will ask an operand to bank 0 one cycle later. Instead, with Barber's Pole layout, the next instruction will likely start its requests from a different bank that depends on the new source register. This uncertainty perturbs the bank access pattern and creates new stalls.

Figure 9 shows this effect. We report the baseline system performance with and without Barber's Pole for `fmatmul`, varying the number of elements. We also report the same

comparison but with CVA6 replaced by the ideal dispatcher. Since the trends are similar, we can focus on the baseline system. Barber's Pole has a positive effect on performance up to 16 double-precision elements (32 Byte per lane), as it increases the number of effective banks used in each lane. From 32 elements (64 Byte/lane, i.e., the effective number of banks is the same as the physical number of banks), the performance is decreased due to the newly introduced conflicts. The longer the vector, the less frequent the introduced stalls happen, as the fetch from the same source registers is not perturbed by Barber's Pole. Barber's Pole effect on performance is mainly driven by the number of Bytes per lane; therefore, shorter data widths will experience the negative effect of this byte layout at higher vector lengths. Since Barber's Pole layout increases the complexity of the hardware that calculates the VRF addresses and can hurt performance when handling long vectors, we decided not to implement it in Ara2.

#### 7.4.2 Main Performance Drivers

To fully characterize Ara2's performance, we studied its behavior when further optimized with modifications that can highly impact its PPA metrics. To amortize the setup time of the internal pipeline when the byte-per-lane ratio is low, Ara2 needs to have larger buffers at each step of its pipeline. We artificially increased the size of the instruction buffers for each internal unit and the number AXI cut-registers from/to Ara's load-store unit. Moreover, we changed the way in which the hazards on the load unit and slide unit are handled, complicating the internal control but allowing for faster hazard resolution. To further decrease the number of stalls, another possible change would be to duplicate the window of simultaneous instructions handled within Ara2 from 8 to 16. All these changes impact the area and timing of a design that requires careful optimizations to balance the timing paths; therefore, they are only used now as a comparison point for more viable solutions presented in Section 9.

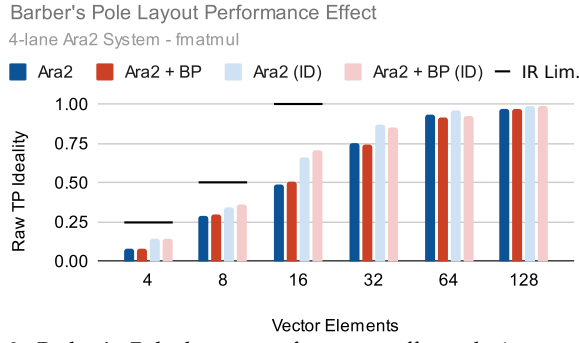


Fig. 9: Barber’s Pole layout performance effects during a matrix multiplication (8 Byte/element). Small benefits exist for shorter vectors, while medium-long vectors suffer from it.

Figure 10 shows the performance of the optimized system compared to the baseline. We also report the system, in both configurations, attached to an ideal dispatcher. The black lines represent the issue-rate limitation, i.e., the intrinsic performance limitation due to the non-ideal rate at which the scalar core issues the vector instructions to Ara. We can see that the optimized system with the ideal dispatcher is not limited by the issue-rate limitation and gets a non-negligible performance boost for a vector 32, 64, and 128 bytes long (up to 32 Byte/lane) if compared with the baseline with the ideal dispatcher and with the current system baseline. On the other hand, we can see that the current system, coupled with CVA6, suffers from multiple problems with short vectors. Namely, the fact that the housekeeping code overhead and the setup time weigh more when the runtime is shorter (smaller problem size).

Figure 11 summarizes the results of the performance analysis, analyzing the various sources of inefficiencies for the current system. Ara’s performance, when dealing with shorter vectors, is limited by multiple factors that depend on the vector length. We merged more contributions when their combined effect was way higher than their effects added (64B, 128B cases). CVA6 highly penalizes the 64B case only if Ara2 is optimized; otherwise, its inefficiencies are hidden by Ara’s ones. We also want to highlight that the CVA6- and Cache-related columns are upper bounds to the system’s performance. Further optimizations would require a heavy re-design of the system, as the most impactful optimizations are the merged ones (violet and orange columns). The effect of the Ara2 inefficiencies on performance drops below 5% from 256B on, demonstrating the computational efficiency of the architecture for medium-long vectors.

## 8 PHYSICAL IMPLEMENTATION

We summarize the system implementation results in Table 3, while Table 4 presents the performance, power, and energy efficiency analysis for a `matmul` on different data types.

Table 5 shows the area breakdown of the system and the cost of supporting arbitrary strides during slide operations compared with the optimized system, which supports only power-of-two strides and time-multiplexes the slide and reshuffle operations, as explained in Section 5. When scaling up, the all-to-all unoptimized (old) slide unit becomes the

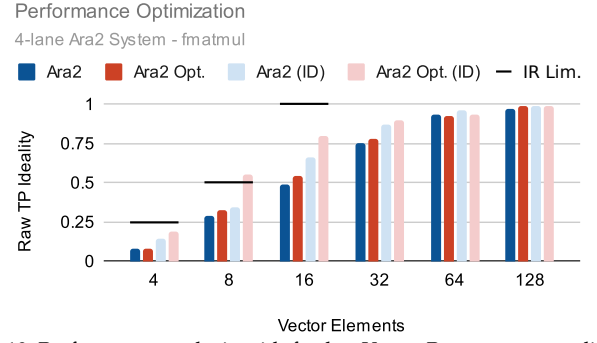


Fig. 10: Performance analysis with further Vector Processor streamlining when executing a matrix multiplication (8 Byte/element). The issue-rate limitation is a hard limit only for the system with CVA6 (opaque lines).

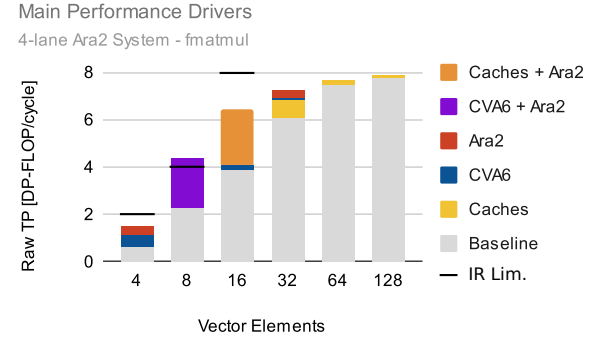


Fig. 11: Main sources of inefficiency. Ara2’s architecture especially limits short vectors from 32 to 128 Byte (up to 32 B/lane), while caches play an important role for 128 and 256 Byte vectors. Kernel: floating-point matrix multiplication (8 Byte/element).

largest non-lane block from four lanes on, growing exponentially with the lanes and dominating the 8-lane design. The mask unit only needs to support reshuffling and generate an enable signal at bit granularity; however, no all-to-all input-to-output byte mapping is required. The load and store units quickly increase their size when scaling up the system but at a lower pace thanks to their limited memory bandwidth ( $4 \times L$  Byte/cycle), which is half of the byte throughput of the main computational units ( $8 \times L$  Byte/cycle) and needs  $\frac{L^2}{2}$  connections. Between these two units, the load unit is the most problematic since its interconnect is duplicated to connect the input AXI memory bytes to the two-entry result queue. The store unit, instead, connects the input register to the AXI bytes directly. The optimized slide unit shows a linear increase, with an area reduction of 83% with respect to the unoptimized one. The greater reduction in area w.r.t. the predicted one can be explained by the diminished routing density that was effectively dominating the unit area. Looking at the 16-lane design with the new slide unit, we see the mask unit and load unit exploding in size and hindering the system’s scalability.

## 9 MULTI-CORE ANALYSIS

In this section, we analyze the performance and energy efficiency trade-off for different system configurations (single-core and multi-core) as a function of the application’s vector length. The analysis from Section 8 suggests that 16 lanes

TABLE 3: Physical implementation metrics in 22nm FD-SOI. In brackets, the increment w.r.t. the same architecture with half the lanes.

Metric (factor)	2 Lanes	4 Lanes	8 Lanes	16 Lanes	16 Lanes*
SS Freq. [GHz]	950	960 (1.0×)	940 (1.0×)	750 (0.8×)	860 (0.9×)
TT Freq. [GHz]	1.35	1.35 (1.0×)	1.35 (1.0×)	1.08 (0.8×)	1.26 (0.9×)
Die Area [mm <sup>2</sup> ]	0.59	0.95 (1.6×)	1.88 (2.0×)	4.47 (2.4×)	4.47 (2.4×)
Cell+Macro Area [kGE]	2291	3688 (1.6×)	6768 (1.8×)	14773 (2.2×)	12864 (1.9×)
Macro Area [kGE]	557	769 (1.4×)	1180 (1.5×)	2010 (1.7×)	2010 (1.7×)
Cell Area [kGE]	1733	2919 (1.7×)	5587 (1.9×)	12763 (2.3×)	10854 (1.9×)
En. Eff.** [FLOPS <sub>DP</sub> /W]	34.1	37.8 (1.1×)	35.7 (0.9×)	—	30.3 (0.8×)

\* No fixed-point support, minimal mask unit.

 \*\*  $f_{matmul}$  between 256x256 matrices, at typical corner

TABLE 4: Performance, power, and energy efficiency for different kernels for a 4-lane design, at 1.35 GHz, in typical conditions, and 2KiB vectors.

Program	Elements	Power [mW]	Performance [GOPS]	Efficiency [GOPS/W]
fmatmul64	256	283	10.7	37.8
fmatmul32	512	238	21.4	90.0
fmatmul16	1024	218	42.8	195.9
imatmul64	256	272	10.4	38.3
imatmul32	512	245	20.9	85.2
imatmul16	1024	231	41.8	181.0
imatmul8	2048	222	83.5	376.0

are a hard limit due to congestion and routing challenges in the all-to-all units of the vector processor. Moreover, a single-core vector processor needs to buffer longer vectors exposed by the application on a single dimension to scale up performance and efficiency when its number of lanes increases, by keeping the same byte-per-lane ratio. However, not all applications expose long vectors on one dimension. A multi-core system offers flexibility in exploiting different parallelization dimensions at the cost of synchronization and memory-transfer overheads, as reported in Figure 13. The experiment includes four systems with the same number of FPU's (16), ranging from a single-core 16-lane Ara2 system to a multi-core system consisting of eight 2-lane Ara2 systems coupled with eight CVA6 instances. The results, depicted in Figures 14, 15, and 16, showcase the raw throughput (FLOP/Cycle), real throughput (FLOPS), and energy efficiency (FLOPS/W) of the various system configurations.

## 9.1 Performance

The *raw throughput* allows for evaluating the system's performance abstracted from the physical implementation. For medium/short vectors (8, 16, 32, 64 64-bit elements), multi-core systems composed of smaller instances outperform those with fewer but larger vector cores. This is due to the exploitation of another dimension of parallelization, allowing

TABLE 5: Ara2's area breakdown and scale-up behavior. In brackets, the area scaling factor w.r.t. the same block in Ara2 with half the lanes. Thanks to the optimization of the SLDU, the MASKU and Vector Load Unit (VLDU) are the main units whose area skyrockets during the system upscaling. When we remove most of the shuffling functions from the MASKU, its area is reduced by 60% in a 16-lane design.

Area [kGE] (factor)	2 Lanes	4 Lanes	8 Lanes	16 Lanes	16 Lanes*
CVA6	894	896 (1.0×)	906 (1.0×)	904 (1.0×)	904 (1.0×)
Lane	612	617 (1.0×)	626 (1.0×)	628 (1.0×)	573 (0.9×)
Dispatcher	16	17 (1.1×)	19 (1.1×)	23 (1.2×)	20 (1.1×)
Sequencer	14	15 (1.1×)	17 (1.2×)	29 (1.6×)	29 (1.6×)
MASKU	38	97 (2.5×)	300 (3.1×)	1105 (3.7×)	442 (1.5×)
ADDRGEN	35	36 (1.0×)	44 (1.2×)	59 (1.3×)	60 (1.4×)
VLDU	15	45 (3.0×)	212 (4.7×)	1286 (6.1×)	1135 (5.4×)
VSTU	8	21 (2.8×)	64 (3.1×)	332 (5.2×)	342 (5.3×)
New SLDU	24	48 (2.0×)	94 (2.0×)	196 (2.1×)	190 (2.1×)
Old SLDU	39	131 (3.4×)	577 (4.4×)	2900 (5.0×)	2860 (5.0×)

\* No fixed-point support, minimal mask unit.

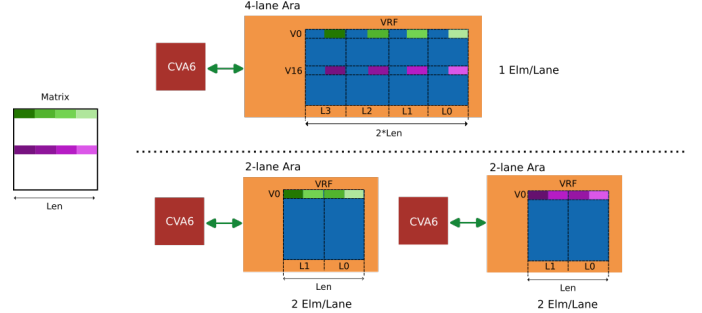


Fig. 13: Comparison of a single-core 4-lane Ara2 system architecture and a two-core architecture made of 2-lane Ara2 processors. Both configurations have 4 FPU's in total. The vector processor can vectorize in one dimension only, while the multi-core system can parallelize multiple dimensions. This allows the multi-core system to reach a higher Byte/Lane ratio when the vectorizable dimension is shorter than the size of a vector register and the application exposes an additional dimension to exploit DLP.

for a byte-per-lane ratio increase. In contrast, as the problem size increases, the FPU's are fully utilized even with the maximum number of lanes. The dual-core 8-lane and single-core 16-lane systems surpass the others at vector lengths of 128 and 256 elements, respectively, as the synchronization overhead and pressure on the memory system decrease with fewer cores. Extremely small problem sizes (8x8x8) suffer from the program setup time because of their lower arithmetic intensity and shorter runtime.

*Issue rate limitation:* Thanks to the RVV specification update, the number of assembly instructions in the main loop of a `matmul` drops from four to three, bringing the issue rate of `vfmacc` instructions from five to four cycles per `vfmacc` (the scalar coefficient can now be forwarded with the `vfmacc`). As shown in Figure 14, this new implicit scalar forwarding contributes to pushing the issue-rate-limitation line [4] to the left. However, the non-ideal issue rate of CVA6 still limits performance for medium-short vectors.

The multi-core vector architecture helps overcome the issue-rate limitation. While the single-core 16-lane Ara2 system cannot theoretically go beyond 16 DP-GFLOP/cycle when operating on 32x32x32 matrices, all the multi-core instances with 16 FPU's exceed this value, with the 8-core 2-lane system reaching 23.6 DP-GFLOP/cycle. This happens since the maximum performance of a 2-lane Ara2 system is lower than the issue-rate limitation. Intuitively, having more scalar cores makes the total issue rate increase, too. Also, a

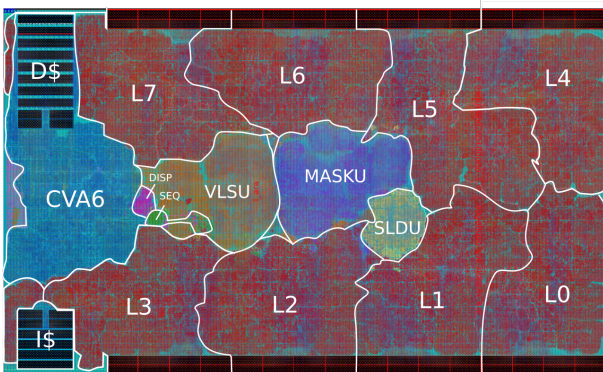


Fig. 12: Floorplan of the 8-lane Ara2 implementation.

multi-core design with smaller Ara2 instances behaves better than a single-core larger Ara2 with the same number of FPUs coupled with an ideal scalar core and memory subsystem, even if the latter system is not affected by the issue-rate limitation. This result is shown in Figure 14.

The previous analysis is valid if the application exposes two dimensions of parallelization. The applications that expose only one parallelizable dimension will always perform better on a single-core larger implementation, as the multi-core architecture will not help increase the byte-per-lane ratio and will pay the synchronization price.

As shown in Figure 15, the overall picture of the system's performance does not change when we take into consideration the real throughput of the various systems by considering the maximum frequencies of the physical implementations for the designs up to 8 lanes. The 16-lane system experiences a non-negligible frequency drop that penalizes the whole computation, which becomes slower than all the other designs for all the different vector lengths.

## 9.2 Energy efficiency

With the multi-core system, we waste the energy of the replicated scalar cores and their memory transfers. This fact is counter-balanced by the different energy efficiencies reached by the physical implementations of the systems with a different lane count. As shown in Section 8, the 4-lane design is the most efficient system, followed by the 8-lane, 2-lane, and 16-lane ones. The multi-core overhead and the different efficiencies of the implementations allow the 4-core 4-lane design to be the most efficient one, reaching more than 39 DP-GFLOPS/W on a  $256 \times 256 \times 256$  problem. The 2-core 8-lane system immediately follows with almost 38 DP-GFLOPS/W on the same problem, thanks to a lower multi-core related power overhead. As expected, the 8-core 2-lane system shows an efficiency from 5% to 18% lower than the 4-core, suffering both from the lower efficiency of the single 2-lane Ara2 systems and the maximum number of cores in the system, with the related overhead. The 16-lane system suffers from the specification update and the additional all-to-all connected unit that degrades the overall energy efficiency. Nevertheless, it overtakes the 8-core 2-lane system on the largest problem size.

In Figures 18 and 19, we present a log-log summary of the previous diagrams. Colors indicate the number of FPUs, and shapes indicate the number of lanes of each Ara2 instance that makes up the multi-core system. The more complex the shape, the higher the number of lanes per core.

The larger systems with fewer cores take over the configurations with smaller cores (simple shapes on the plot) when the number of FPUs is constant (same color on the plot) when the vector length is increased, meaning that having more lanes in the single instances is more beneficial with longer vectors, as we noticed before.

The plots show that for smaller vectors, many smaller vector processors are better than a large one that cannot effectively exploit all the dimensions of parallelism present in the application. If we take this to the limit, we see that with extremely short vectors (i.e., 1 or 2 elements), having a vector processor does not make sense, and a multi-core CVA6 scalar system would be more performant and efficient.

## 10 COMPARISON WITH SOA

### 10.1 Performance

As already noticed in Section 1, it is not easy to compare our performance metrics with the SoA since the benchmarking is often done on a very limited number of kernels and because the software implementation is not available. Moreover, the metrics are not always clearly defined. In [5], we could not find the definition of the throughput metric and the lengths of the application vectors. For this reason, we assume them to be the longest possible, i.e., at least 256 DP-Elements per vector (256 Byte/Lane). The 8-lane Ara2 system is almost as performant as Vitruvius+ even with a  $80KiB/32KiB = 2.5\times$  smaller VRF and no register-renaming features. Indeed, it gets the same performance for `matmul` and `pathfinder`, while Ara2's FFT is  $1.3\times$  faster even for a lower byte-per-lane ratio (128 against 256). `jacobi2d`'s performance is hard to compare as it is unclear how the authors calculated the throughput metric, getting more than what we consider the maximum throughput for that kernel (8 DP-FLOP/cycle). Ara2's performance for `fmatmul`, `fconv2d` gains a  $1.1\times$  boost compared to [4] thanks to the frequency gain. Other than that, the comparison with Hwacha done in [4] is still valid, as no updated results have been published.

The comparison with Vicuna [9] is especially hard since it is a 32-bit integer-only vector core. Its medium and fast configurations have the same computational capabilities, in terms of total throughput, of a 2-lane and 16-lane Ara2 systems. The reported utilization results are relative to two 8-bit `fmatmul` whose sizes are comparable with a  $256 \times 32 \times 256$  and a  $1024 \times 128 \times 1024$  64-bit `fmatmul` problems. Our results refer to  $32 \times 32 \times 32$  and  $128 \times 128 \times 128$  matrices, and this makes the comparison unfair, as increasing the other two dimensions boosts the utilization. Nevertheless, the 2-lane Ara2 system shows virtually the same utilization. Our 16-lane system, instead, lags behind ( $\sim 30\%$  vs.  $\sim 60\%$ ), especially when executing the smaller problem. This is mainly due to the size of Ara's D-Cache,  $16\times$  smaller than Vicuna's in the same configuration. Spatz [12], an integer vector processor coupled with Snitch [28], is able to reach almost 70% utilization with eight cores and 2 Image Processing Units (IPUs) per core, while Ara2 reaches 30% for the same problem size. However, Spatz is a 32-bit integer-only vector architecture, and all the benchmark data are kept in the low latency L1 memory, which eliminates miss-related stalls.

### 10.2 Power, Performance, Area

The novel Ara2 architecture boosts the design's operational frequency up to 15% (i.e., 8 lanes) compared to Ara [4], with a critical path of  $\sim 40$  FO4 inverter delays for the 4-lane design. Its area is 2%, 7%, 15%, and 37% higher than Ara with 2, 4, 8, and 16 lanes, respectively. This is due to the newly introduced functionality, coupled with a  $4\times$  size reduction of the VRF. The MASKU, introduced to keep the architecture compliant with RVV, decreases the implementation efficiency of the whole design starting from 8 lanes and a visible area, and energy-efficiency degradation hinders a further scale-up. Further study on the MASKU and VLDU is needed to reduce their footprint without hitting the system's performance. E.g., the data of the VLDU can be aligned before entering the system, easing the routing in the unit. On the other



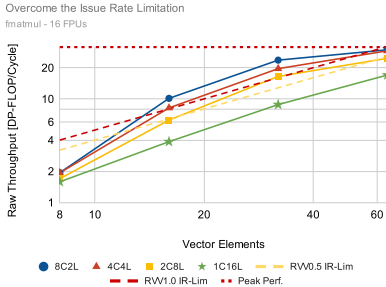


Fig. 14: A multi-core implementation helps overcome the issue-rate limitation for small vectors (*fmatmul*).

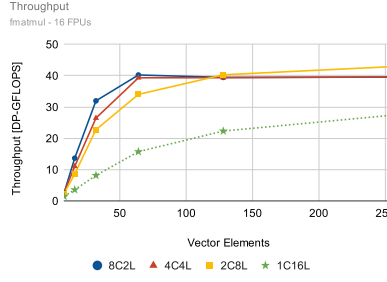


Fig. 15: Multi- and single-core throughput for different 16-FPU configurations of the Ara2 system in typical conditions (*fmatmul*).

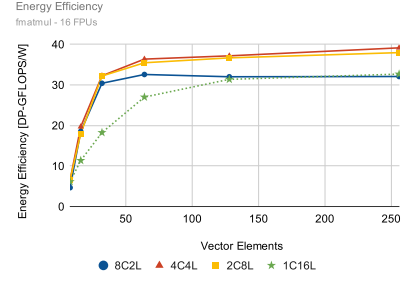


Fig. 16: Multi- and single-core energy efficiency for different 16-FPU configurations of the Ara2 system in typical conditions (*fmatmul*).

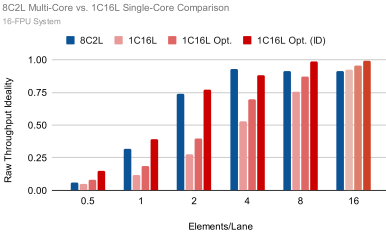


Fig. 17: Performance comparison of multi- and single-core 16-FPU Systems (*fmatmul*). In the last column of each set, CVA6 is replaced by the Ideal Dispatcher.

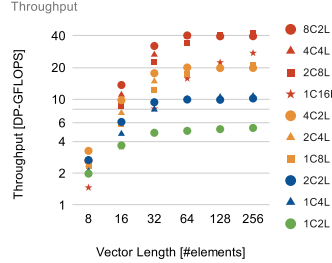


Fig. 18: Throughput comparison of single- and multi-core vector architectures with 2, 4, 8, and 16 FPU's (*fmatmul*).

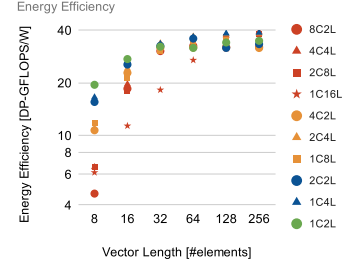


Fig. 19: Energy Efficiency comparison of single- and multi-core vector architectures with 2, 4, 8, and 16 FPU's (*fmatmul*).

hand, a complete 8-lane Ara2 system (CVA6, Ara2, scalar caches) reaches virtually the same frequency and area as a Vitruvius+ instance alone without the scalar core and memories (1.4 GHz, 1.3 mm<sup>2</sup>) [5].

Comparing the energy efficiency across different implementations is hard due to the sensitivity that the power consumption has with respect to the input data distribution. E.g., executing the same 256x256x256 *fmatmul* kernel on our 4-lane Ara2 System can lead to energy efficiencies from 38.8 to 65 GFLOPS<sub>DP</sub>/W depending on the input distribution. Using a normal distribution with mean 0 and variance 1, instead of a uniform one between [0,1], also leads to a 7.5% power difference. In this scenario, comparing our energy efficiency with Vitruvius+ is hard, as the paper does not report the used input number distribution, and it is not clear if the power figures consider the scalar core and memories too, as we do. Moreover, we could not reproduce the number reported in their comparison tables. A comparison with Spatz is also nontrivial, as the architecture is a 32-bit integer only, leading to substantially lower power figures.

## 11 CONCLUSION

In this work, we presented Ara2, the first open-source RVV 1.0 vector architecture. We implement the design with 2, 4, 8, and 16 lanes in 22nm FD-SOI technology and reach 1.35 GHz (for 8 and fewer lanes) thanks to a new lightweight SLDU able to reduce the number of interconnect wiring and hardware of the all-to-all byte-connected unit by 70%. For compliance with RVV, Ara2 requires a new all-to-all connected MASKU to support the modified VRF layout of

the mask vectors, complicating the physical implementation. This, together with the newly supported features like floating-point reductions, make the 4-lane configuration become the most efficient design point, with an SoA energy efficiency of almost 39 GFLOPS<sub>DP</sub>/W during a matrix multiplication.

The flexible Ara2 architecture reaches, on average, more than 50% of its throughput ideality starting from 128 Bytes per lane on the whole benchmark pool with every system configuration. Furthermore, with only a 64 byte-per-lane ratio, it achieves more than 75% of its maximum throughput on the most crucial kernels like matrix multiplications and convolutions and more than 90% from 128 Byte/Lane. We also investigate the detrimental impact of the Barber's Pole layout on long-vector performance and thoroughly analyze the primary performance drivers of the vector architecture, including the scalar core and its memory system.

To overcome the issue-rate performance limitation, we evaluate multi-core vector architectures, which show that smaller vector core instances can boost the performance of applications that expose more than one dimension of parallelization (e.g., *matmul*), especially when the vectorizable dimension cannot provide high byte-per-lane ratios, with performance improvements up to 3x when compared to a single-core architecture with the same overall computation capability. This is especially beneficial when the system cannot exploit the advantages of long vectors, e.g., when the application does not expose them on a single dimension.

## ACKNOWLEDGMENTS

This work was supported by the ETH Future Computing Laboratory (EFCL), financed by a gift from Huawei Technolo-



gies, and by the TRISTAN (101095947) project that received funding from the HORIZON KDT-JU programme.

## REFERENCES

- [1] R. M. Russell, "The CRAY-1 computer system," *Commun. ACM*, vol. 21, no. 1, p. 63–72, 1978.
- [2] Fujitsu, "How world-first technology is unleashing higher processing speeds for AI's ever-rising computational needs," 2020. [Online]. Available: <https://corporate-blog.global.fujitsu.com/fgb/2020-02-03/how-world-first-technology-is-unleashing-higher-processing-speeds-for-ai-s-ever-rising-computational-needs/>
- [3] J. Ma *et al.*, "An analytical framework for estimating scale-out and scale-up power efficiency of heterogeneous manycores," *IEEE Transactions on Computers*, vol. 65, no. 2, pp. 367–381, 2016.
- [4] M. Cavalcante *et al.*, "Ara: A 1-GHz+ scalable and energy-efficient RISC-V vector processor with multiprecision floating-point support in 22-nm FD-SOI," *IEEE Transactions on Very Large Scale Integration*, vol. 28, no. 2, pp. 530–543, 2020.
- [5] F. Minervini *et al.*, "Vitruvius+: An area-efficient RISC-V decoupled vector coprocessor for high performance computing applications," *ACM Trans. Archit. Code Optim.*, vol. 20, no. 2, pp. 1–25, 2023.
- [6] R. Espasa, "Introducing SemiDynamics high bandwidth RISC-V IP cores," RISC-V Global Forum 2020, 2020. [Online]. Available: <https://www.european-processor-initiative.eu/wp-content/uploads/2021/03/202012.RISC-V-SUMMIT.pdf>
- [7] I. A. Assir *et al.*, "Arrow: A RISC-V vector accelerator for machine learning inference," *arXiv preprint arXiv:2107.07169*, 2021.
- [8] SiFive Intelligence X280, SiFive Corp., San Mateo, CA, USA, 2022, revision 21G3. [Online]. Available: [https://sifive.cdn.prismic.io/sifive/62e0df53-be02-4b50-b211-aa55b7042fc8\\_x280-datasheet-21G3.pdf](https://sifive.cdn.prismic.io/sifive/62e0df53-be02-4b50-b211-aa55b7042fc8_x280-datasheet-21G3.pdf)
- [9] M. Platzer and P. Puschner, "Vicuna: A timing-predictable RISC-V vector coprocessor for scalable parallel computation," in *33rd ECRTS*, ser. LIPIcs, vol. 196. Schloss Dagstuhl, 2021, pp. 1:1–1:18.
- [10] C. Chen, X. Xiang *et al.*, "Xuantie-910: A commercial multi-core 12-stage pipeline out-of-order 64-bit high performance RISC-V processor with vector extension: Industrial product," in *ISCA'20*, 2020, pp. 52–64.
- [11] AndesCore NX27V, Andes Technology, Hsinchu City, Taiwan, 2020. [Online]. Available: <http://www.andestech.com/en/products-solutions/andescore-processors/riscv-nx27v>
- [12] M. Cavalcante *et al.*, "Spatz: A compact vector processing unit for high-performance and energy-efficient shared-L1 clusters," in *ICCAD'22*. ACM, Oct. 2022, pp. 1–9.
- [13] SiFive Performance P270, SiFive Corp., San Mateo, CA, USA, 2022, revision 21G3. [Online]. Available: [https://sifive.cdn.prismic.io/sifive/859c28c0-8bd5-4fc4-9113-a25a2a89bf9c\\_P270+Data+Sheet.pdf](https://sifive.cdn.prismic.io/sifive/859c28c0-8bd5-4fc4-9113-a25a2a89bf9c_P270+Data+Sheet.pdf)
- [14] SiFive, "P870 high-performance RISC-V processor," in *Hot Chips: A Symposium on High-Perf. Chips*. IEEE, Aug. 2023.
- [15] C. Ramírez *et al.*, "A RISC-V simulator and benchmark suite for designing and evaluating vector architectures," *ACM Trans. Archit. Code Optim.*, vol. 17, no. 4, pp. 1–30, 2020.
- [16] H. T. Kung, "Memory requirements for balanced computer architectures," *SIGARCH Comp. Arch. News*, vol. 14, no. 2, May 1986.
- [17] P. Vizcaino *et al.*, "Short reasons for long vectors in HPC CPUs: a study based on RISC-V," *arXiv preprint arXiv:2309.06865*, 2023.
- [18] M. Johns and T. J. Kazmierski, "A minimal risc-v vector processor for embedded systems," in *FDL'20*, 2020, pp. 1–4.
- [19] K. Patsidis *et al.*, "RISC-V2: A scalable RISC-V vector processor," in *ISCAS'20*, 2020, pp. 1–5.
- [20] C. Schmidt *et al.*, "An eight-core 1.44-GHz RISC-V vector processor in 16-nm FinFET," *IEEE Journal of Solid-State Circuits*, vol. 57, no. 1, pp. 140–152, 2022.
- [21] —, *RISC-V Vector Extension Proposal*, 2015. [Online]. Available: <https://riscv.org/wp-content/uploads/2015/06/riscv-vector-workshop-june2015.pdf>
- [22] Krste Asanovic, *Vector Extension Proposal v0.2*, 2016. [Online]. Available: <https://riscv.org/wp-content/uploads/2016/12/Wed0930-RISC-V-Vectors-Asanovic-UC-Berkeley-SiFive.pdf>
- [23] K. Asanovic *et al.*, *The RISC-V Vector ISA*, 2017. [Online]. Available: <https://riscv.org/wp-content/uploads/2017/12/Wed-1330-RISCVRogerEspasaVEXT-v4.pdf>
- [24] —, *RISC-V Vector Extension Proposal*, 2018. [Online]. Available: <https://riscv.org/wp-content/uploads/2018/05/15.20-15.55-18.05.06.VEXT-bcn-v1.pdf>
- [25] —, *RISC-V Vector Extension Proposal*, 2020. [Online]. Available: <https://github.com/riscv/riscv-v-spec/releases/tag/0.9>
- [26] L. Bertaccini, L. Benini, and F. Conti, "To buffer, or not to buffer? a case study on FFT accelerators for ultra-low-power multicore clusters," in *ASAP'21*, 2021, pp. 1–8.
- [27] Cristóbal Ramírez Lazo, "RiVec benchmark suite." [Online]. Available: <https://github.com/RALC88/riscv-vectorized-benchmark-suite>
- [28] F. Zaruba *et al.*, "Snitch: A tiny pseudo dual-issue processor for area and energy efficient execution of floating-point intensive workloads," *IEEE Transactions on Computers*, vol. 70, no. 11, pp. 1845–1860, 2020.



**Matteo Perotti** received his M.Sc. degree in Electronic Engineering from the Polytechnic University of Turin, Italy, in 2019. He is currently pursuing a Ph.D. degree at the Integrated Systems Laboratory of ETH Zurich, Switzerland, under the supervision of Prof. Luca Benini. Matteo's research interests include highly efficient computing architectures, vector processing, computation with high dynamic-range data types, and the RISC-V ecosystem in general.



**Matheus Cavalcante** received his M.Sc. degree in Integrated Electronic Systems from the Grenoble Institute of Technology (Phelma) in 2018, and his Ph.D. from ETH Zurich in 2023. During his Ph.D. studies, Matheus worked with the Digital Circuits and Systems Group under the supervision of Prof. Luca Benini. Matheus' research interests include vector processing, large-scale high-performance computer architectures, and emerging VLSI technologies.



**Renzo Andri** received the B.Sc., M.Sc. and Ph.D. degree in Electrical Engineering and Information Technology at ETH Zurich in 2013, 2015, and 2020, respectively. Since 2020 he is working at the Huawei Research Center Zurich. His research focuses lies on energy-efficient machine learning acceleration and processor design down to full-custom IC design including hardware-algorithm codesign. In 2019, he won the IEEE TCAD Donald O. Pederson Award.



**Lukas Cavigelli** received the d Ph.D. degree in electrical engineering and information technology from ETH Zurich in 2019. After a year as a Post-doc at ETH Zurich, he has joined Huawei's Zurich Research Center in Spring 2020. His research interests include deep learning, computer vision, embedded systems, and low-power integrated circuit design. He has received several best paper awards including the IEEE TCAD Donald O. Pederson award in 2019.



**Luca Benini** holds the chair of Digital Circuits and Systems at ETH Zurich and is Full Professor at the Università di Bologna. He received a Ph.D. from Stanford University. Dr. Benini's research interests are in energy-efficient parallel computing systems, smart sensing micro-systems and ML hardware. He is a Fellow of the ACM and a member of the Academia Europaea. He received the IEEE Mac Van Valkenburg Award in 2016, the ACM/IEEE A. Richard Newton Award in 2020, and the IEEE E. McCluskey Award in 2023.